MODELLING HYDRODYNAMIC STABILITY IN ELECTROCHEMICAL CELLS

José Pontes – jopontes@metalmat.ufrj.br
Metallurgy and Materials Engineering Department – Federal University of Rio de Janeiro
P.O. Box 68505, Rio de Janeiro, RJ, 21941-972 Brazil
Norberto Mangiavacchi – norberto.mangiavacchi@gmail.com
Group of Environmental Studies of Hydropower Reservoirs (GESAR Group),
State University of Rio de Janeiro,
R. Fonseca Telles 524, Rio de Janeiro, RJ, 20550-013 Brazil
Gustavo Rabello dos Anjos – gustavo.rabello@gmail.com
Group of Environmental Simulations of Hydropower Reservoirs (GESAR Group),
State University of Rio de Janeiro,
R. Fonseca Telles 524, Rio de Janeiro, RJ, 20550-013 Brazil

Abstract. *We review the key points concerning the linear stability of the classical von Kármán's solution of rotating disk flow, modified by the coupling, through the fluid viscosity, with concentration field of a chemical species. The results were recently published by Mangiavacchi* et al. *(*Phys. Fluids, **19***: 114109, 2007) and refer to electrochemical cells employing iron rotating disk electrodes, which dissolve in the 1* $\mathbf{M}$ $\mathbf{H_2SO_4}$ *solution of the electrolyte. Polarization curves obtained in such cells present a current instability at the beginning of the region where the current is controlled by the the hydrodynamics. The onset of the instability occurs in a range of potentials applied to the cell and disappear above and below this range. Dissolution of the iron electrode gives rise to a thin concentration boundary layer, with thickness of about 4% of the thickness of the hydrodynamic boundary layer. The concentration boundary layer increases the interfacial fluid viscoity, diminishes the diffusion coefficient and couples both fields, with a net result of affecting the hydrodynamic of the problem. Since the current is proportional to the interfacial concentration gradient of the chemical species responsible by the ions transport, the instability of the coupled fields can lead to the current instability observed in the experimental setups. This work presents the results of the linear stabilituy analysis of the coupled fields and the first results concerning the Direct Numerical Simulation, currently undertaken in our group. The results show that small increases of the intrefacial viscosity result in a significant reduction of the stability of modes existing in similar configurations, but with constant viscosity fluids. Upon increasing the interfacial viscosity, a new unstable region emerges, in a range of Reynolds numbers much smaller than the lower limit of the unstable region previously known. Though the growth rate of modes in the previously known region is larger than the one of modes in the new region, the amplitude of the concentration unstable modes in this one is very large when compared to the amplitude of the associated hydrodynamic unstable modes. In addition concentration modes are always confined in a rather thin region, leading to the existence of large intrerfacial concentration gradient. Concentration modes in the new unstable region seem thus, to have a combination of properties sufficient to drive detectable current oscillations. The numerical experiments show that a progressive increase in the interfacial viscosity initially reduces the stability of the flow, but an increase beyond a certain limit restores the stability properties of constant viscosity flows.*

1. Posing the Problem

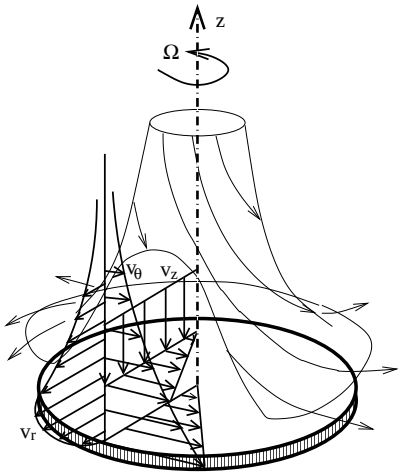

Figure 1: Von Kármán's flow close to the axis of a rotating disk.

The hydrodynamic field developed close to the axis of a large rotating disk belongs to the restricted class of problems admitting a analytical or semi-analytical similarity solution of the hydrodynamic equations. The angular velocity imposed to the fluid at the surface gives rise to a centrifugal effect and to a radial flow outwards. Continuity requires that the flow be replaced by an incoming one that approaches the disk. Close to the surface, the axial velocity of the incoming flow is reduced and the centrifugal effect appears. This is the region of the hydrodynamic boundary layer. The steady tri-dimensional solution of this flow was found by Von Kármán (1932) and is schematically shown in Fig. 1.

The boundary layer becomes unstable beyond a critical Reynolds number. The first stabilitiy studies of Von Kármán's solution are due to Smith (1946)) [14], who found the emergence of spirals as shown in Fig. 2. The pattern may turn with the disk angular velocity or other. When turnning slower than the disk, the spirals arms tend to bend in the upstream direction. The pattern is "pushed" by the mean flow. Patterns bending downstream, or consisting of radial straight lines or either of circumferences are also possible. The coexistence of spirals bending in the up and the downstream directions was observed by Moisy (2004) [11], in a setup of two counter rotating disks.

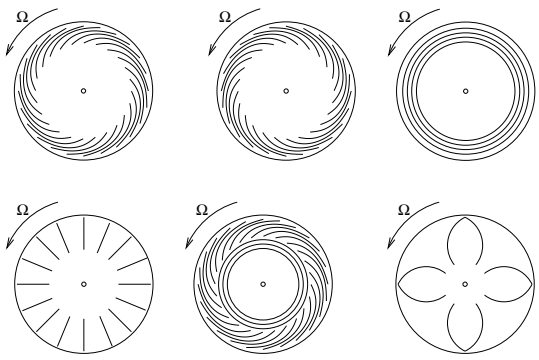

Figure 2: Possible perturbation patterns emerging after the first instability of von Kármán's solution.

Gregory *et al.* (1955) [4] measured the critical Reynolds number beyond which Von Kármán's solution becomes unstable and proposed the first theoretical approach to the stability problem, not taking into account viscosity effects. Stability studies conducted after the eighties were mainly made in groups interested in the effect of a secondary cross flow, on the stability of a main one, as those found in swept wings. Rotating disk flow presents certain characteristics also found in swept wings. In swept wings the upstream flow is decomposed in a component perpendicular to the wing, responsible by the lift and a cross component that antecipates the transition to turbulence. In rotating disk flow, a secondary radial flow appears in consequence of the imposed azimuthal velocity at the interfce. Thanks to Von Kármán's exact solution and to the more controlled conditions found in rotating disks than in wings, rotating disks became a prototype to infer on the instabilization mechanisms occuring in swept wings. Malik (1986) [8] evaluated the first neutral curve of perturbations turnning with the angular velocity of the disk (stationary perturbations). The critical Reynolds number was found sa 285.36. Lingwoood (1995) [7] extended Malik's results by considering non-stationary perturbations, turning with angular velocity different of the disk velocity and found critical Reynolds numbers on the order of 80. In addition, Lingwood addressed the absolute stability problem. The flow becomes absolutely unstable when the a perturbation originated in a point is carried by the angular ve-

locity of the flow and returns to the origin point before being completely damped and excites again the remaining pertubation at that point.

Stability studies conducted after 1990 focused on compressible fluid configurations, having in mind the fact that swept wings operate in the high subsonic regime.

The question of rotating disk flow stabilility appears also in electrochemical problems. Electrochemical cells employing a rotating disk electrode are widely used due to the relatively simple setup and to the fact that the mass flow at the electrode/electrolyte interface is independent of the radial position. The rate of transfer of ions is conveniently controled by the the angular velocity imposed to the electrode. Fig. 3 schematically shows a typical arrangement of these cells, with three electrodes. The counter electrode consists of a platinum screen placed along the cell wall to assure an uniform distribution of the electric potential. Potentials are measured against the reference electrode. The working electrode consists of a $5\,mm$ diameter iron rod covered with a $10\,mm$ diamenter resin cast, except in the base, through which the current flows. The electrode is coupled to a variable velocity electric motor. Typical electrode velocites range from 100 to $900\,rpm$.

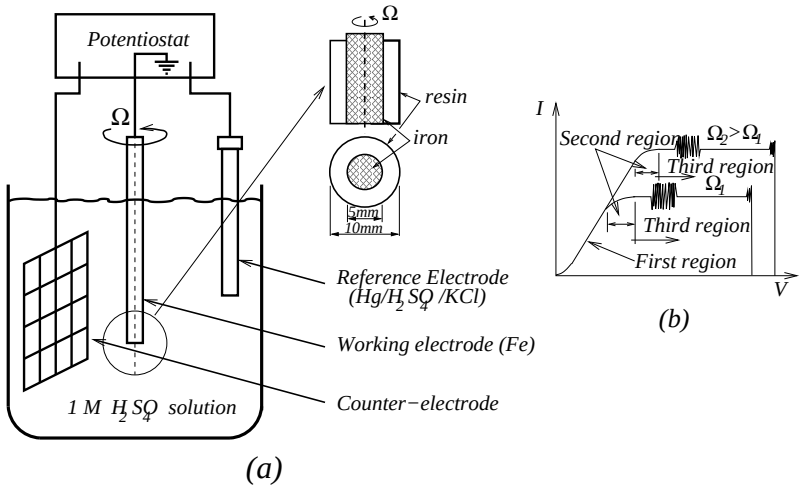

Figure 3: An elecrtochemical cell with a rotating disk electrode (a) and the polarization curve showing the three regions (b).

Polarization curves experimentally obtained in the dissolution of iron electrodes in $\mathbf{H_2SO_4}$ electrolytes present three regions (Barcia *et al.*, 1992 [1]). The first one occurs at reletively low overvoltages applied to the working electrode. The current is approximately proportional to the overvoltage and depends on the dissolution process. The current is not affected by transport phenomena occuring in the electrolyte, like the angular velocity imposed to the working electrode. Polarization curves show a second region, where the current depends on the applied overvoltage and also on the hydrodynamics, which is defined by the electrode angular velocity. By further increasing the overvoltage, a current *plateau* appears in the polariaztion curves, where the current depends only on the angular velocity of the electrode, and no longer, on the overvoltage. The overvoltage level of the *plateau* is proportional to $\Omega^{1/2}$.

The hydrodynamic field at the base of the working electrode is approximated by Von Kármán's similarity solution. This hypothesis is justified by the thickness of the hydrodynamic boundary layer, which is proportional to $\Omega^{1/2}$, ranging from 0.5 to $1.3\,mm$, being thus one order of magnitude smaller than the $10\,mm$ electrode diameter. Dissolution of the iron electrode gives raise to a $\mathbf{F}e^{+2}$ ions concentration boundary layer. The ratio between the hydrodynamic and the concentration boundary layers is given by $\delta_h/\delta_c \approx 2\,Sc^{1/3}$ (Levich. 1962 [6]), where Sc is the Schmidt number. Typical Schmidt numbers in electrochemical cells is 2000, resulting in concentration boundary layers with thicknesses of order of 4% of the thickness of the hydrodynamic one.

The concentration boundary layer leads to a reduction of the iron diffusion coefficient in the electrolyte. The Stokes-Einstein law postulates that the product of the diffusion coefficient by the electrolyte viscosity is constant, implying in a visosity increase at the interface. The

effect couples both fields.

The cell current may be evaluated through the ions transfer at the electrode/electrolyte interface, which is due to two effects: ions concentration gradient ($i \propto dC/dz|_{z=0}$) and ions migration due to the electric field. Barcia *et al.* (1992) [1] showed that the concentraion gradient is the dominant effect, what leads to the concluison that the current depends on the spatial distribution of a relevant chemical species, that in turn, depends on the hydrodynamic field. Instabilities of the hydrodynamic field and of the interfcial concentration gradient may thus be responsible for the current oscillations observed in the current *plateau*. However, Reynolds numbers attained in elctrochemical cells are of order of 20 – 40, being thus clearly smaller than critical experimental values found in the literature and the theoretical values found by Malik and by Lingwood.

This work deals with the coupling of the hydrodynamcic field, to the concentration one of a chemical species responsible by the current. Three questions are posed: (a) if the the coupling changes the stability properties of the purely hydrodynamic field, reducing the critical Reynolds numbewr to the range of values attained in electrochemical setups, (b) if possible oscillations of the interfacial concentration gradient are strong enough to drive the current oscillations experimentaly observed and (c) what mechanisms lead to the suppression of the cuurent instability beyond a certain overvoltage level. The results herein presented support a positive answer to the first question, suggest that the hydrodynamic instability of the coupled fields is strong enough to drive the current oscillation, but still do not explain the instability suppresion.

2. Governing Equations

The problem is governed by the continuity and the Navier-Stokes equations, coupled through the viscosity, to the transport equation of the relevant chemical species. These equations, written in the frame attached to the surface of the rotating disk read:

$$\operatorname{div} \mathbf{v} = 0 \tag{1}$$

$$\frac{D\mathbf{v}}{Dt} = -2\boldsymbol{\Omega} \times \mathbf{v} - \boldsymbol{\Omega} \times (\boldsymbol{\Omega} \times \mathbf{r}) - \frac{1}{\rho} \mathbf{grad}\, p + \frac{1}{\rho} \operatorname{div} \tau \tag{2}$$

$$\frac{D\mathcal{C}}{Dt} = \operatorname{div}(\mathcal{D}\, \mathbf{grad}\, \mathcal{C}) \tag{3}$$

where $\boldsymbol{\Omega}$ is the angular velocity of the rotating disk electrode, $\mathcal{C}$ and $\mathcal{D}$ are, respectively, the concentration and the diffusion coefficient of the representative chemical species and τ is the viscous stress tensor for a newtonian fluid with the viscosity depending on the concentration of the chemical species.

The evolution equations are rewritten in non-dimensional form. Variables having units of length or its reciprocal (radial and axial coordinates, perturbation wavenumber along the radial direction) are made non-dimensional with the length used to measure the thickness of the boundary layer, $(\nu_\infty/\Omega)^{1/2}$, where ν_∞ is the bulk viscosity of the fluid. Velocity components are divided by the local imposed azimuthal velocity $r_e\Omega$, pressure is divided by $\rho(r_e\Omega)^2$, viscosity is divided by the bulk viscosity, ν_∞, time and the eigenvalue of the linearized problem are made non-dimensional with the time required by a particle, turning with the azimuthal velocity $r_e\Omega$, to move a distance equal to the reference length, $(\nu_\infty/\Omega)^{1/2}$. Here, r_e is the dimensional coordinate along the radial direction at which the stability analysis will be carried out. The non-dimensional concentration of the chemical species is defined by:

$$C = \frac{\mathcal{C} - \mathcal{C}_\infty}{\mathcal{C}_S - \mathcal{C}_\infty} \tag{4}$$

where $\mathcal{C}_S$ and $\mathcal{C}_\infty$ are, respectively, the concentration of the chemical species at the electrode surface and in the bulk. We define also the Reynolds and the Schmidt numbers by the relations:

$$R = r_e \left(\frac{\Omega}{\nu_\infty} \right)^{1/2} \qquad \text{and} \qquad Sc = \frac{\mathcal{D}_\infty}{\nu_\infty} \tag{5}$$

The Reynolds number may be seen as a nondimensional distance to the disk axis. At this point, we assume that the viscosity depends on the non-dimensional concentration of the chemical species according to:

$$\nu = \nu_\infty \exp(mC) \tag{6}$$

where m is a non-dimensional parameter depending on the electrochemical characteristics of the system (electrode material, type of electrolyte, applied potential), but not on the concentration of the chemical species. In particular, this parameter defines the interface viscosity, given by $\nu = \nu_\infty \exp(m)$. This equation is based on a thermodynamic model proposed by Esteves *et al.* (2001) [2]. We also assume the Stokes-Einstein law:

$$\mathcal{D}\nu = \mathcal{D}_\infty \, \nu_\infty \tag{7}$$

where $\mathcal{D}_\infty$ is the bulk diffusion coefficient. Using the bulk coefficients to rewrite Eqs. 7 and 6 in non-dimensional form, we obtain:

$$\mathcal{D}\nu = 1 \qquad \text{and} \qquad \nu = \exp(mC) \tag{8}$$

Equations 1 – 3 are rewritten as follows, in non-dimensional form:

$$\operatorname{div} \mathbf{v} = 0 \tag{9}$$

$$\frac{D\mathbf{v}}{Dt} = -2\,\mathbf{e}_z \times \mathbf{v} - \mathbf{e}_z \times (\mathbf{e}_z \times r\,\mathbf{e}_r) - \mathbf{grad}\, p + \frac{1}{R} \operatorname{div} \tau \tag{10}$$

$$\frac{DC}{Dt} = \frac{1}{R\,Sc} \operatorname{div}(\mathcal{D}\,\mathbf{grad}\, C) \tag{11}$$

A destabilizing potential of the coupling between the hydrodynamic and the chemical species fields can be seen in Eq. (11): the Reynolds number is amplified by the Schmidt number, which takes here the value $Sc = 2000$, typical for electrochemical cells.

3. The Base State

3.1 Base State Equations

The base state is the von Kármán similarity solution for a fluid with the viscosity depending on the concentration field, which is assumed to vary along the axial coordinate only.

$$\begin{pmatrix} \bar{v}_r \\ \bar{v}_\theta \\ \bar{v}_z \\ \bar{p} \\ \bar{\mathcal{C}} \end{pmatrix} = \begin{pmatrix} r\,\Omega\,F(z) \\ r\,\Omega\,G(z) \\ (\nu_\infty\,\Omega)^{1/2}\; H(z) \\ \rho\nu_\infty\Omega\,P(z) \\ \mathcal{C}_\infty + (\mathcal{C}_S - \mathcal{C}_\infty)\,C(z) \end{pmatrix} \tag{12}$$

All variables in Eq. 12 are dimensional, except the axial dependent profiles, F, G, H, C and the axial coordinate z. Boundary conditions for F, G, H and P are $F = G = H = P = 0$

at the disk surface $(z = 0)$, $F = H' = 0$ and $G' = -1$ as $z \longrightarrow \infty$. The non-dimensional concentration profile, C, varies from 1, at $z = 0$, to 0, as $z \longrightarrow \infty$.

Introducing Eq. 12 and the constitutive equations of the stress tensor Eqs. **??** – **??** in Eqs. 1 – 3, together with Eqs. (6) and 7, we obtain the ordinary nonlinear system for the axial profiles F, G, H, P and C:

$$2F + H' = 0 \tag{13}$$

$$F^2 - (G+1)^2 + HF' - \nu F'' - \nu' F' = 0 \tag{14}$$

$$2F(G+1) + HG' - \nu G'' - \nu' G' = 0 \tag{15}$$

$$P' + HH' - \nu H'' - 2\nu' H' = 0 \tag{16}$$

$$Sc\, HC' - \frac{C''}{\nu} + \frac{\nu'}{\nu^2} C' = 0 \tag{17}$$

where prime denotes derivatives with respect to the non-dimensional axial coordinate z. The viscosity ν and its derivatives are written in non-dimensional form.

3.2 Evaluation of the Viscosity at the Electrode/Electrolyte Interface

Solving Eqs. 13 – 17 requires specification of two parameters: the bulk Schmidt number and the parameter m appearing in Eq. 6, which ultimately defines the electrolyte viscosity at the interface with the electrode. At this point, we assume that the limit current density at the interface is proportional to the concentration gradient of the relevant chemical species generated by the dissolution of the electrode. Ions migration due to the potential gradient is neglected. The current density is given by the relation (Barcia, 1992 [1]):

$$\frac{i}{n\mathcal{F}\dfrac{1}{Sc}\dfrac{1}{\nu_0/\nu_\infty}\left(\mathcal{C}_\infty - \mathcal{C}_s\right)\sqrt{\nu_\infty \Omega}} = \left.\frac{dC}{dz}\right|_{z=0} \tag{18}$$

where i is expressed in A/cm^2, n is the valence number of the chemical species $(n = 2)$, $\mathcal{F} = 96500\, C/mol$, is the Faraday constant, $\mathcal{C}_s = 2.0 \times 10^{-3} mol/cm^3$ is the dimensional concentration of the species at the electrode interface (saturated condition), $\mathcal{C}_\infty = 0\, mol/cm^3$ and ν_0 is the fluid viscosity at the interface. The limit current density obtained experimentally is $i = 0.8810\, A/cm^2$ at $900\, rpm$ (Geraldo, 1998 [3]).

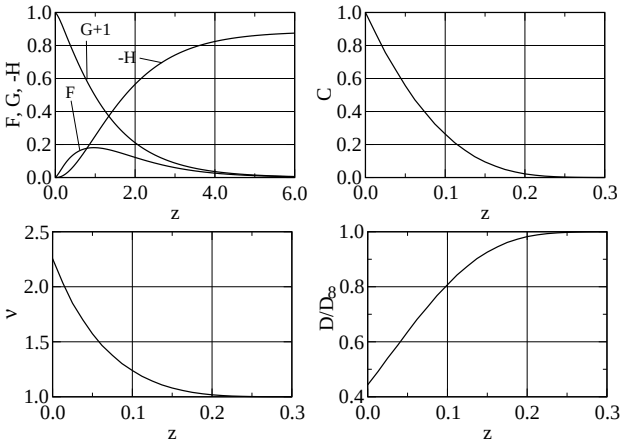

Figure 4: Stationary dimensionless velocity, concentration, viscosity and diffusion, profiles, F, G, H and C for $\nu_0/\nu_\infty = 2.255$ and $Sc = 2000$.

An initial value is specified for m, Eqs. 13 – 17 are solved. The ratio ν_0/ν_∞ is evaluated and the non-dimensional normal derivative of the concentration at the interface, $dC/dz|_{z=0}$, is obtained from the profiles. These figures are introduced in Eq. 18, leading to a value for the current density. The value initially specified for m is corrected and the procedure is repeated until convergence to the experimental value of i is reached. At convergence we obtain $\nu_0/\nu_\infty = 2.255$.

3.3 Base State Profiles

The non-dimensional velocity, concentration, viscosity and diffusion coeffi-

cient profiles, F, G, H, C, ν and $\mathcal{D}$, obtained for $\nu_0/\nu_\infty = 2.255$ and $Sc = 2000$ are shown in Fig. 4.

The thin concentration boundary layer, results in velocity profiles very close to the ones obtained for the constant viscosity case. In particular, we obtain $H = -0.88559$ far from the disk for the variable viscosity flow considered, a figure slightly different from the asymptotic value for the constant viscosity case, $H = -0.88447$. However, the derivatives of the velocity profiles are strongly affected inside the concentration boundary layer, as shown in Fig. 5.

4. Stability of the Base State

4.1 Stability Equations

We turn now to the question of the stability of the base state with respect to small disturbances. The hydrodynamic and chemical fields are written as a sum of the base state plus a perturbation:

$$\left.\begin{array}{rcl} v_r &=& \bar{v}_r + \tilde{v}_r \\ v_\theta &=& \bar{v}_\theta + \tilde{v}_\theta \\ v_z &=& \bar{v}_r + \tilde{v}_z \\ p &=& \bar{p} + \tilde{p} \\ \mathcal{C}_T &=& \bar{\mathcal{C}} + \tilde{\mathcal{C}} \end{array}\right\} \qquad (19)$$

where the perturbation, in dimensional form, is given by:

$$\begin{pmatrix} \tilde{v}_r \\ \tilde{v}_\theta \\ \tilde{v}_z \\ \tilde{p} \\ \tilde{\mathcal{C}} \end{pmatrix} = \begin{pmatrix} r_e\Omega\, f \\ r_e\Omega\, g \\ r_e\Omega\, h \\ \rho\nu_\infty\Omega\, \pi \\ (\mathcal{C}_s - \mathcal{C}_\infty)\, c \end{pmatrix} \times \exp\left[i(\alpha r + \beta R\theta - \omega t)\right] + cc. \qquad (20)$$

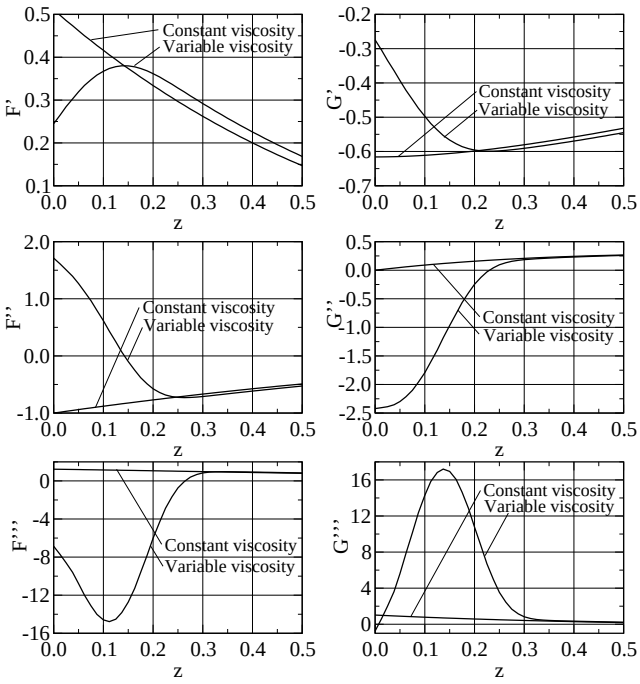

Figure 5: The first three derivatives of the non-dimensional velocity profiles, F and G, for the constant and variable viscosity cases, with $\nu_0/\nu_\infty = 2.255$ and $Sc = 2000$.

Here ω is a complex number, with $\Re(\omega)$ and $\Im(\omega)$ being, respectively, the frequency and the rate of growth of the perturbation. The functions f, g, h, π and c depend on the axial coordinate z and the parameters α and β are the components of the perturbation wave-vector along the radial and azimuthal directions. For a given time, the phase of the perturbation is constant along branches of a logarithmic spiral, with the branches curved in the clockwise direction if β/α is positive and counter-clockwise, if negative. The structure turns counter-clockwise if $\Re(\omega)/\beta$ is positive and clockwise, if negative.

The base state and the perturbation variables are rewritten in no-dimensional form, introduced in Eqs. 9 – 11 and nonlinear terms are dropped. Perturbation variables are not, strictly speaking, separable since the resulting equations for the profiles f, g, h, π and c still contain the radial coordinate r. In order to overcome the problem it is necessary to make the *parallel flow* assumption, where it is assumed that variations of the above profiles are small as far as $\Delta r/r \ll 1$. This approximation holds whenever the stability analysis is carried sufficiently far from $r = 0$. If variations of the profiles with r are small, this coordinate can be assumed as

constant. The non-dimensional constant r is the Reynolds number at which the stability analysis is carried. This is the parallel flow hypothesis. Adoption of this hypothesis in rotating disk flow[9, 15, 7], is made by replacing r by R.

To conclude, terms of order R^{-2} are dropped, leading to a generalized complex non-symmetric eigenvalue-eigenfunction problem in the form:

$$\begin{pmatrix} A_{11} & A_{12} & A_{13} \\ A_{21} & A_{22} & A_{23} \\ A_{31} & & A_{33} \end{pmatrix} \begin{pmatrix} h \\ \eta \\ c \end{pmatrix} = \omega R \begin{pmatrix} B_{11} & & \\ & B_{22} & \\ & & B_{33} \end{pmatrix} \begin{pmatrix} h \\ \eta \\ c \end{pmatrix} \tag{21}$$

where $\eta = \alpha g - \beta f$, missing elements in the matrices are zero and the operators A_{ij} and B_{ij} are given by:

$$\begin{array}{llllll} A_{11} = a_{114}D^4 + a_{113}D^3 + a_{112}D^2 + a_{111}D + a_{110} & & & & A_{12} = a_{121}D + a_{120} \\ A_{13} = a_{132}D^2 + a_{131}D + a_{130} & & & & \\ A_{21} = a_{211}D + a_{210} & A_{22} = a_{222}D^2 + a_{221}D + a_{220} & & & A_{23} = a_{231}D + a_{230} \\ A_{31} = a_{310} & A_{33} = a_{332}D^2 + a_{331}D + a_{330} & & & \\ & & & & \\ B_{11} = D^2 - \bar{\lambda}^2 & B_{22} = 1 & & & B_{33} = iSc \end{array}$$

where $D^n = d^n/dz^n$. By defining $\lambda^2 = \alpha^2 + \beta^2$, $\bar{\alpha} = \alpha - i/R$ and $\bar{\lambda}^2 = \alpha\bar{\alpha} + \beta^2$ we obtain for the coefficients a_{ijk}:

$$\begin{aligned}
&a_{114} = i\nu \quad a_{113} = i(2\nu' - H) \quad a_{112} = i\nu'' - i\nu\left(\lambda^2 + \bar{\lambda}^2\right) + R\left(\alpha F + \beta G\right) - i\left(H' + F\right) \\
&a_{111} = -i\nu'\left(\lambda^2 + \bar{\lambda}^2\right) + iH\bar{\lambda}^2 \\
&a_{110} = i\bar{\lambda}^2\left(\nu'' + \nu\lambda^2\right) - R\left(\alpha F + \beta G\right)\bar{\lambda}^2 - R\left(\bar{\alpha}F'' + \beta G''\right) + iH'\bar{\lambda}^2 \\
&a_{121} = 2\left(G + 1\right) \qquad a_{120} = 2G' \\
&a_{132} = R\left(\bar{\alpha}F' + \beta G'\right)\gamma \qquad a_{131} = \left[2R\left(\bar{\alpha}F'' + \beta G''\right) + 6i\bar{\lambda}^2 F\right]\gamma + 2R\left(\bar{\alpha}F' + \beta G'\right)\gamma' \\
&a_{130} = \left[R\bar{\lambda}^2\left(\alpha F' + \beta G'\right) + R\left(\bar{\alpha}F''' + \beta G'''\right) + 4i\bar{\lambda}^2 F'\right]\gamma \\
&\qquad + \left[2R\left(\bar{\alpha}F'' + \beta G''\right) + 6i\bar{\lambda}^2 F\right]\gamma' + R\left(\bar{\alpha}F' + \beta G'\right)\gamma'' \\
&a_{211} = 2\left(G + 1\right) \qquad a_{210} = -iR\left(\alpha G' - \beta F'\right) \\
&a_{222} = i\nu \quad a_{221} = i\left(\nu' - H\right) \quad a_{220} = -i\nu\lambda^2 + R\left(\alpha F + \beta G\right) - iF \\
&a_{231} = iR\left(\alpha G' - \beta F'\right)\gamma \qquad a_{230} = iR\left[\left(\alpha G'' - \beta F''\right)\gamma + \left(\alpha G' - \beta F'\right)\gamma'\right] \\
&a_{310} = R\,Sc\,C' \\
&a_{332} = -\frac{1}{\bar{\nu}} \qquad a_{331} = \frac{1}{\bar{\nu}}\left(\frac{\bar{\nu}'}{\bar{\nu}} + \frac{1}{\bar{\nu}}C'\gamma + Sc\,\bar{\nu}H\right) \\
&a_{330} = iR\,Sc\left(\alpha F + \beta G\right) - \frac{1}{\bar{\nu}}\left\{-\bar{\lambda}^2 + \frac{1}{\bar{\nu}}\left[\left(2\frac{\bar{\nu}'}{\bar{\nu}}\gamma - \gamma'\right)C' - \gamma C''\right]\right\}
\end{aligned}$$

where $\gamma = d\nu/dC$. Boundary conditions of the problem require non-slip flow, vanishing axial component of the velocity and saturation concentration of the chemical species at the electrode surface. These conditions are already fulfilled by the base-state and cannot be modified by the perturbation. In consequence we require $h = \eta = c = 0$ in $z = 0$. Moreover, continuity requires that $h' = 0$ at the interface. In $z \longrightarrow \infty$ we require that the perturbation vanishes $(h = h' = \eta = c = 0)$.

4.2 Stationary Neutral and Unstable Level Curves

The neutral stability curves for stationary disturbances $[\Re(\omega) = 0]$, obtained by solving the eigenvalue-eigenfunction problem for $Sc = 2000$ and $\nu_0/\nu_\infty = 2.255$, are presented in Fig. 6.

This figure shows that the coupling enlarges the unstable region of constant viscosity fluids to a wider range of wave-numbers and to a critical Reynolds number of order of 50% of the critical wavenumber of constant viscosity fluids. Fig. 6 shows also the existence of a new family of much more unstable modes. Critical Reynolds numbers of this region are in the range of the ones attained in experimental setups. We refer to these new modes as *chemical* and to modes belonging to the former family as *hydrodynamic*.

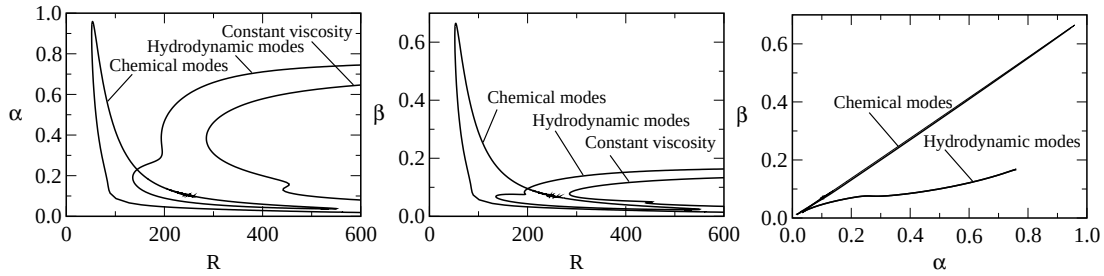

Figure 6: Neutral stability curves of stationary perturbations, in the $\alpha \times R$, $\beta \times R$ and $\alpha \times \beta$ planes.

The enlarged unstable hydrodynamic region suggests that modes inside this region might possibly have larger growth rates (ω_i) than unstable modes of constant viscosity fluids. Similarly, we could expect that the narrow region of unstable chemical modes could not allow for the existence of modes with large growth rates. This is the case, indeed. Figure (7) shows neutral and level curves evaluated for positive rates of growth for fluids with constant viscosity on left, for the unstable region of hydrodynamic and chemical modes at the center and right, respectively.

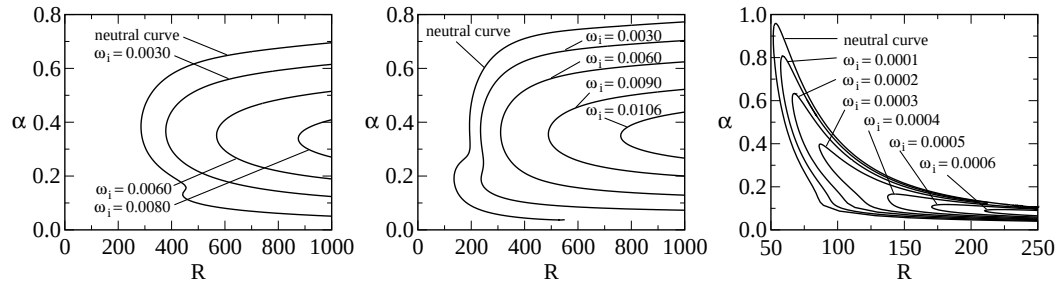

Figure 7: Neutral and level curves with positive growth rates (ω_i) of fluids with constant viscosity (on left) and in the unstable region of hydrodynamic (at the center) and chemical modes (on right) of the variable viscosity case.

An analysis of Fig. 7 shows that growth rates of hydrodynamic modes of variable viscosity fluids attaint values up to 30% larger than in the case of constant viscosity case. However, growth rates of chemical modes are more than one order of magnitude smaller than those of hydrodynamic modes.

4.3 Marginally Stable Eigenmodes – Hydrodynamic and Chemical Unstable Regions

Despite of the low growth rate, unstable modes in the chemical region show a combiation of properties that seem capable to drive the current oscillations observed in experiemtal setups. Fig. 8 shows the hydrodynamic and chemical concentration components of a mode on the neutral curve of the chemical region (first row) and on the neutral curve of hydordynamic region (second row). The amplitude of the chmical component is of same order of the hydrodynamic components in the second case but significantly larger in the case of modes in the chemical region. In addition, the chemical component is always confined to a narrow region close to the

interface, leading to high values of the interfacial concentration gradient. This gradient seems sufficiently strong to drive detectable current oscillations.

4.4 Effects of Decoupling the Transport of the Chemical Species and of Variation of the Interfcial Viscosity

Numerical experiments cnducted by the authors Mangiavacchi *at al.*, 2007 [10] show that the coupling, and not the viscosity stratification is responsible for the existence of the new chemical region of unstable modes, for the enlargement and reduction of the critical Reynolds number of the hydrodynamic region. The experiment was done by setting operators $A_{13} = A_{23} = 0$ in Eq. 21.

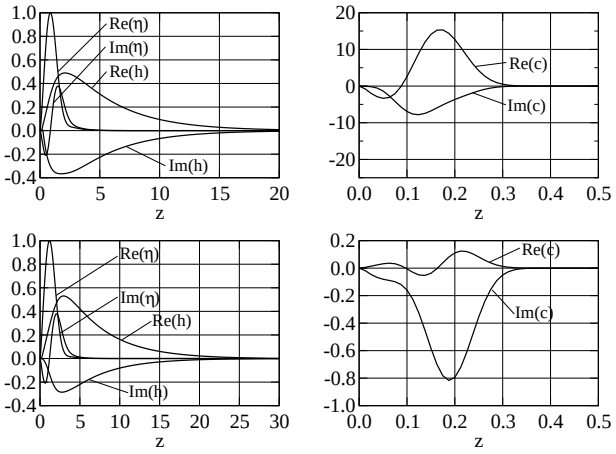

Figure 8: Real and imaginary parts of one modes on the neutral curve of the chemical region, at the point $R = 156.99$, $\alpha = 0.20124$, $\beta = 0.13767$, in the first row and of a mode on the neutral curve of the hydrodynamic region, at the point $R = 135.48$, $\alpha = 0.18726$, $\beta = 0.067182$ (second row).

The authors also showed that a progressive increase of the interfacial viscosity results firstly, in a decrease of the overall satbility, but, as the viscosity increases the destabilizing effect is inversed and the stability properties of constant viscosity fields are restored. The $\nu_0/\nu_\infty = 2.255$ is not the most unstable one. An increase by 5% of the interfacial viscosity enlarges the area of the unstable hydrodynamic region to practically its maximum. A narrow new unstble region already exists with a 2% increase in the interfacial viscosity, but with a critical Reynolds number of order of 1100. As the interfacial viscosity increases the area of the unstable chemical region increases and moves to inner radius. The area attains a maximum at $\nu_0/\nu_\infty \approx 1.5$. Further increasing the interfacial viscosity reduces the area of the unstable chemical region. The region disappears close to $\nu_0/\nu_\infty = 2.8$. New increases in the interfacial viscosity reduce the hydrodynamic unstable region to the one of constant viscosity fluids.

5. Direct Numerical Simulation

The linear stability analysis identifies the distance from the electrode axis, below which perturbations introduced in Von Kármán's solution are damped. Perturbations with geometry within a range that is enlarged as the distance of the axis increases are amplified. The linear analysis identifies the stability limit but does answer questions on the unstable modes first selected. Selection is made through the nonlinear coupling, when the amplitude of unstable modes is sufficiently large to trigger interaction mechanisms. The nonlinear interaction leads to the selection of one or the few modes of the first emerging unstable pattern. The study of pattern selection is done by following the evolution and the interaction of a small number of prescribed modes, close to a bifurcation point. An alternative method consists in doing a three-dimensional direct numerical simulation. This is the method we currently follow. A FEM code has been developed [5, 12, 16], with the following characteristics: pressure and diffusive terms are treated by a Galerkin method, convective terms are treated in a semi-lagrangean form in order to assure the necessary stability to the code. Time is discretized according to a first order

forward differences scheme, leading to a system in the form:

$$M(\frac{\mathbf{v}_i^{n+1} - \mathbf{v}_d^n}{\Delta t}) + \frac{1}{R} K \mathbf{v}^{n+1} - G p^{n+1} = 0 \tag{22}$$

$$D\mathbf{v}^{n+1} = 0 \tag{23}$$

$$M_c(\frac{c_i^{n+1} - c_d^n}{\Delta t}) + \frac{1}{R\,Sc} K_c c^{n+1} = 0 \tag{24}$$

where M and M_c are mass operators, K and K_c are the momemtum and concentration diffusion operators, G and D are the gradient and divergent operators. The hydrodynamics is solved first and the results are used to evaluate the concentration of the chemical species. Upon rewritting the hydrodynamic equations in matrix form, we obtain:

$$\begin{bmatrix} B & -\Delta t\,\mathbf{G} \\ \mathbf{D} & \mathbf{0} \end{bmatrix} \begin{bmatrix} \mathbf{u}^{n+1} \\ \mathbf{p}^{n+1} \end{bmatrix} = \begin{bmatrix} \mathbf{r}^n \\ \mathbf{0} \end{bmatrix} + \begin{bmatrix} \mathbf{bc}_1 \\ \mathbf{bc}_2 \end{bmatrix} \tag{25}$$

where $B = \mathbf{M} + (\Delta t/R)\,\mathbf{K}$. The LHS matrix in Eq. 25 is factorized as follows:

$$\begin{aligned} \begin{bmatrix} B & -\Delta t\,\mathbf{G} \\ \mathbf{D} & \mathbf{0} \end{bmatrix} &= \begin{bmatrix} \mathbf{B} & \mathbf{0} \\ \mathbf{D} & \Delta t\,\mathbf{D}B^{-1}\mathbf{G} \end{bmatrix} \begin{bmatrix} \mathbf{I} & -\Delta t\,B^{-1}\mathbf{G} \\ \mathbf{0} & \mathbf{I} \end{bmatrix} \\ &\approx \begin{bmatrix} \mathbf{B} & \mathbf{0} \\ \mathbf{D} & \Delta t\,\mathbf{D}B_L^{-1}\mathbf{G} \end{bmatrix} \begin{bmatrix} \mathbf{I} & -\Delta t\,B_L^{-1}\mathbf{G} \\ \mathbf{0} & \mathbf{I} \end{bmatrix} \end{aligned} \tag{26}$$

The resulting linear systems are solved by a projection method. The application of the projection method decouples the velocity and pressure fields computations, resulting in two symmetric and positive definite matrices that are solved by the preconditioned conjugate gradient method. A reverse Cuthill-McKee reordering and an incomplete Cholesky preconditioning scheme are applied to solve the linear systems efficiently. Cubic tetrahedral elements are employed, pressure is evaluated at the vertices and the velocity, at the vertices and the centroid of the element (mini-element). Variables from the previous time step are used to evaluate the chemical species field, decoupling the hydrodynamics from the scalar variable transport.

Fig. 9 shows results of the FEM simulations: the velocity profiles for constant viscosity, first figure, and for variable viscosity, second figure. The results agree with the analytical von Kármán solution [13]. The boundary layer for the variable viscosity is thicker than the constant viscosity case, and presents an additional inflection point, increasing thus the instability of the profile.

The FEM code is now validated and will be employed for the simulation of the nonlinear evolution of the most unstable modes found in the linear analysis.

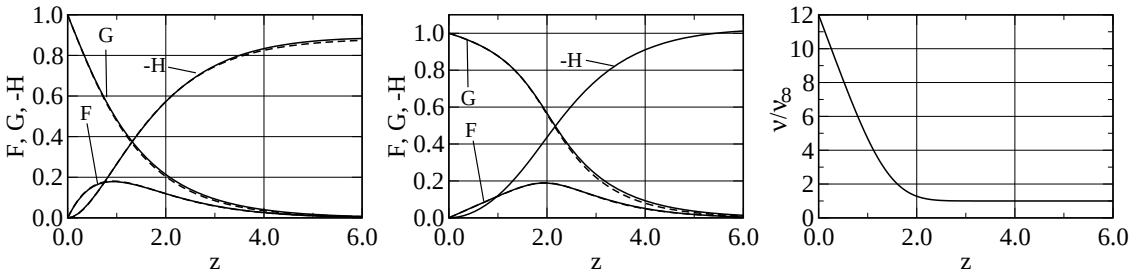

Figure 9: Steady hydrodynamic profiles for constant viscosity fluids (on left) and for fluids with the viscosity depending on the axial coordinate z (at the cenetr). Full lines refer to the FEM solution and dashed lines to the solution of Von Kármán's equations. The right pannel shows the steady viscosity profile used to evaluate the velocity profiles in the central pannel.

REFERENCES

[1] O. E. Barcia, O. R. Mattos, and B. Tribollet. Anodic dissolution of iron in acid sulfate under mass transport control. *J. Eletrochem. Soc.*, 139:446–453, 1992.

[2] M. J. C. Esteves, M. J. E. M. Cardoso, and E. Barcia. A Debye-Hückel model for calculating the viscosity of binary strrong electrolyte solutions,. *Ind. Eng. Chem. Res.*, 40:5021–5028, 2001.

[3] A. B. Geraldo, O. E. Barcia, O. R. Mattos, F. Huet, and B. Tribollet. New results concerning the oscillations observed for the system iron-sulphuric acid. *Electrochim. Acta*, 44:455–465, 1998.

[4] N. Gregory, J. T. Stuart, and W. S. Walker. On the stability of three-dimensional boundary layers with application to the flow due to a rotating disk. *Phil. Trans. Roy. Soc. London*, A-248:155–199, 1955.

[5] T. Hughes and A. Brooks. *A theoretical framework for Petrov-Glaerkin methods with discontinuous weighting functions: application to the streamline upwind procedure*. Wiley, 1982.

[6] V. G. Levich. *Physicochemical Hydrodynamics*. Prentice Hall, Englewood Cliffs, NJ, 1962.

[7] R. J. Lingwood. Absolute instability of the boundary layer on a rotating disk. *J. Fluid Mech.*, 299:17–33, 1995.

[8] M. R. Malik. The neutral curve for stationary disturbances in rotating-disk flow. *J. Fluid Mech.*, 164:275–287, 1986.

[9] M. R. Malik, Wilkinson, and S. A. Orzag. Instability and transition in a rotating disk. *AIAA J.*, 19-9:1131–1138, 1981.

[10] N. Mangiavacchi, J. Pontes, O. E. Barcia, O. E. Mattos, and B. Tribollet. Rotating disk flow stability in electrochemical cells: Effect of the transport of a chemical species. *Phys. Fluids*, 19:114109, 2007.

[11] F. Moisy, O. Doaré, T. Passuto, O. Daube, and M. Rabaud. Experimental and numerical study of the shear layer instability between two counter-rotting disks. *J. Fluid Mech.*, 507:175–202, 2004.

[12] O. Pironneau. *Finite Element Methods for Flows*. Wiley, 1989.

[13] H. Schlichting and K. Gersten. *Boundary Layer Theory*. Springer, Berlin, 1999.

[14] N. Smith. Exploratory investigation of laminar boundary layer oscillations on a rotating disk. Technical Report TN-1227, NACA, Dec. 1946.

[15] S. Wilkinson and M. R. Malik. Stability experiments in the flow over a rotating disk. *AIAA J.*, 23:588, 1985.

[16] O. C. Zienkiewicz and R. L. Taylo. *The Finite Element Method for Fluids Dynamics*. Wiley, 2000.